Human Molecular Genetics, 2015, Vol. 24, No. 9 2492–2507

doi: 10.1093/hmg/ddv010
Advance Access Publication Date: 18 January 2015
Original Article

ORIGINAL ARTICLE

An ER-directed gelsolin nanobody targets the first step in amyloid formation in a gelsolin amyloidosis mouse model

Wouter Van Overbeke[1], Jantana Wongsantichon[5,†], Inge Everaert[2,†], Adriaan Verhelle[1], Olivier Zwaenepoel[1], Anantasak Loonchanta[6], Leslie D. Burtnick[6], Ariane De Ganck[1,‡], Tino Hochepied[7,3], Jody Haigh[3,9,10], Claude Cuvelier[4], Wim Derave[2], Robert C. Robinson[5,8,*] and Jan Gettemans[1,*]

[1]Department of Biochemistry, Faculty of Medicine and Health Sciences, [2]Department of Movement and Sport Sciences, Faculty of Medicine and Health Sciences, [3]Department of Biomedical Molecular Biology and [4]Department of Pathology, Faculty of Medicine and Health Sciences, Ghent University, Ghent, Belgium, [5]Institute of Molecular and Cellular Biology, A*STAR, Biopolis, Singapore 138673, Singapore, [6]Department of Chemistry and Centre for Blood Research, Life Sciences Institute, University of British Columbia, Vancouver, British Columbia, Canada, [7]Department for Molecular Biomedical Research, VIB, Ghent, Belgium, [8]Department of Biochemistry, National University of Singapore, 8 Medical Drive, Singapore 117597, Singapore, [9]Vascular Cell Biology Unit, VIB Inflammation Research Centre, Ghent, Belgium and [10]Mammalian Functional Genetics Laboratory, Division of Blood Cancers, Australian Centre for Blood Diseases, Department of Clinical Haematology, Monash University and Alfred Health Centre, Melbourne, Australia

*To whom correspondence should be addressed. Email: jan.gettemans@ugent.be (J.G.) or rrobinson@imcb.a-star.edu.sg (R.C.R)

Abstract

Hereditary gelsolin amyloidosis is an autosomal dominantly inherited amyloid disorder. A point mutation in the *GSN* gene (G654A being the most common one) results in disturbed calcium binding by the second gelsolin domain (G2). As a result, the folding of G2 is hampered, rendering the mutant plasma gelsolin susceptible to a proteolytic cascade. Consecutive cleavage by furin and MT1-MMP-like proteases generates 8 and 5 kDa amyloidogenic peptides that cause neurological, ophthalmological and dermatological findings. To this day, no specific treatment is available to counter the pathogenesis. Using GSN nanobody 11 as a molecular chaperone, we aimed to protect mutant plasma gelsolin from furin proteolysis in the *trans*-Golgi network. We report a transgenic, GSN nanobody 11 secreting mouse that was used for crossbreeding with gelsolin amyloidosis mice. Insertion of the therapeutic nanobody gene into the gelsolin amyloidosis mouse genome resulted in improved muscle contractility. X-ray crystal structure determination of the gelsolin G2:Nb11 complex revealed that Nb11 does not directly block the furin cleavage site. We conclude that nanobodies can be used to shield substrates from aberrant proteolysis and this approach might establish a novel therapeutic strategy in amyloid diseases.

[†] J.W. and I.E. contributed equally to this work.
[‡] Present address: Biogazelle, Ghent, Belgium.

Received: November 4, 2014. **Revised:** January 9, 2015. **Accepted:** January 14, 2015

Introduction

Amyloid-forming proteins are associated with over 30 diseases, some of which are prevalent neurodegenerative disorders such as Alzheimer's, Huntington's and Parkinson's disease (1). Protein homeostasis in these diseases is defective and conformational changes result in β-sheet structures with a high propensity to aggregate. As a result, fibrous structures form deposits in the tissues, leading to clinical symptoms of various natures. Over the last decade, the importance of intermediate aggregated states has been realized. These intermediates have been shown to be more toxic to the cells than the amyloid fibrils and consequently might be the source of amyloid pathology (2,3). Gelsolin amyloidosis or Familial amyloidosis-Finnish type (FAF) is a rare autosomal, dominant disease in which secretion of gelsolin fragments causes amyloid formation (4,5). A mutation in the *GSN* gene (G654A/T is the most common one) results in misfolding and subsequent aberrant proteolysis of plasma gelsolin. Gelsolin is a calcium-regulated, actin-binding protein involved in severing of F-actin filaments (6). Calcium regulation is imperative for accurate functioning of gelsolin and ensures proper folding of wild-type gelsolin that is normally unaffected by aberrant proteolysis (7). Mutant gelsolin (D187N/Y) loses calcium regulation, which results in improper folding of the G2 domain (8–10). Mutant G2, with a perturbed conformation, exposes a furin cleavage site at its surface that is normally buried in the wild-type structure. The mutant, secreted variant of gelsolin encounters furin in the *trans*-Golgi network and undergoes proteolysis (11). As a consequence, the two fragments of mutant gelsolin are secreted. The 68 kDa C-terminal part (C68) is important in the further pathological process because it acts as a substrate for further pathological proteolysis. Upon secretion and entrance into the extracellular matrix, C68 is cleaved by MT1-MMP like proteases that give rise to 8 and 5 kDa peptides (12). These peptides are amyloidogenic and result in plaque formation in multiple tissues of affected patients. Upon disease progression, the overall clinical presentation is a triad of neurological, ophthalmological and dermatological findings (13), further signs of abnormalities in other organs may occur. There is no specific treatment available to counter gelsolin amyloidosis pathogenesis. Instead, symptomatic treatments are used to improve quality of life for the patients. Several therapeutic strategies have been suggested, aiming for inhibition of protease activity (12,14,15). However, undesired side effects are to be expected when these proteases are inhibited. Here, we aimed for substrate protection using nanobodies. Nanobodies (or VHHs) are single-domain antibodies, discovered as the variable part of the heavy chain of heavy chain antibodies in Camelidae (16). Nanobodies are endowed with properties advantageous towards biotechnological and medical applications (17–21). We have recently shown that nanobodies raised against the 8 kDa amyloidogenic fragment are able to reduce gelsolin buildup following intraperitoneal injection in gelsolin amyloidosis mice (22). In the present study, we used a distinct gelsolin nanobody to shield mutant plasma gelsolin from pathological furin proteolysis. Furin is a membrane-associated proprotein convertase that is ubiquitously expressed and found in all vertebrates and in many invertebrates (23). Furin catalyzes the proteolytic maturation of proprotein substrates in the secretory pathway (24), activates pathogenic agents (25,26) and has an essential role in embryogenesis (27). The proprotein convertase localizes to the *trans*-Golgi network and undergoes highly regulated dynamic cycling to endosomes and the cell surface (24). The minimal consensus site cleaved by furin is Arg-X-X-Arg↓ (25), a site that is present in gelsolin as ^{169}Arg-Val-Val-Arg^{172}. We show that GSN Nb11 specifically hinders gelsolin degradation by furin, *in vitro* as well as when the nanobody is targeted to the endoplasmic reticulum of HEK293T cells. X-ray crystal structure determination of the gelsolin G2:Nb11 complex revealed that Nb11 does not directly block the furin cleavage site. GSN Nb11 showed no cross-reaction with mouse gelsolin, favoring its application in the gelsolin amyloidosis mouse model (28). We therefore raised transgenic mice, designed in such a manner that they secrete GSN Nb11 into the circulation. These mice were crossed with gelsolin amyloidosis homozygotes to generate offspring that express both mutant plasma gelsolin and GSN Nb11. In these mice, we observed a reduced aberrant gelsolin staining pattern in skeletal muscle tissue and consequently, these mice displayed improved muscle contractile properties when compared with littermate controls. We show here that gelsolin nanobodies can be used to protect mutant plasma gelsolin from pathological furin proteolysis and in this manner, counter amyloidogenesis at an early stage.

Results

Gelsolin Nb11 reduces furin proteolysis of mutant plasma gelsolin *in vitro*

In a previous study in our lab, different classes of gelsolin nanobodies were characterized and used as intrabodies in cancer cell lines (18). Epitope mapping and ITC data enabled us to set up a strategy where we aim to prevent furin proteolysis of mutant plasma gelsolin. The epitope of GSN Nb11 resides in gelsolin domain 2 (^{137}G – ^{247}L) (18,29), encompassing the region where furin proteolyzes mutant plasma gelsolin (^{169}RVVR^{172}↓). We hypothesized that binding of this nanobody to mutant plasma gelsolin might interfere with furin proteolysis (Fig. 1A). GSN Nb13, interacting with gelsolin domains 4–5 (distant to the furin cleavage site), was chosen to validate the specificity of GSN Nb11 on furin proteolysis (Fig. 1B). Both GSN Nb11 and GSN Nb13 were reported to have binding affinities for cytoplasmic gelsolin in the low nanomolar range: 1.00 ± 0.11 nM and 9.26 ± 1.61 nM, respectively (in the presence of calcium) (18). The affinity of these nanobodies for *mutant* plasma gelsolin (PG*) was also determined in the presence of calcium and found to be similar (Supplementary material, Fig. S1A and B). For GSN Nb11, the affinity for PG* was one order of magnitude lower when compared with cytoplasmic GSN, likely due to the mutation in G2 (where the GSN Nb11 epitope resides) (Supplementary material, Fig. S1C).

As a first step to verify our hypothesis, we performed an *in vitro* furin cleavage assay (Fig. 2A). Recombinant mutant plasma gelsolin was incubated with GSN Nb11/13 prior to degradation by furin. In the presence of GSN Nb11 (Fig. 2A, upper panels), we observed reduced proteolysis of full-length plasma gelsolin as the molar ratio of Nb: gelsolin increased. Quantification revealed a C68 signal reduction of 34% ($P < 0.01$) when GSN Nb11 was added in an equimolar concentration (Fig. 2B). In contrast, GSN Nb13 (Fig. 2A, lower panels) had no influence on furin activity; no statistically significant differences were observed upon quantification of the C68 signal (Fig. 2B). We tested the persistence of the GSN Nb11 effect over time and observed that a ×2 molar excess of GSN Nb11 manages to strongly reduce furin proteolysis up to 8 h after adding the recombinant furin (Fig. 2C). GSN Nb11 also had no influence on the C68 proteolysis by MT1-MMP, a matrix metalloprotease cleaving the ^{243}M-^{244}L scissile bond in G2 (Supplementary material, Fig. S2). This further confirms the specificity of GSN Nb11 regarding the furin inhibition. The ability of GSN Nb11 to bind C68 (with a truncated G2 domain) was

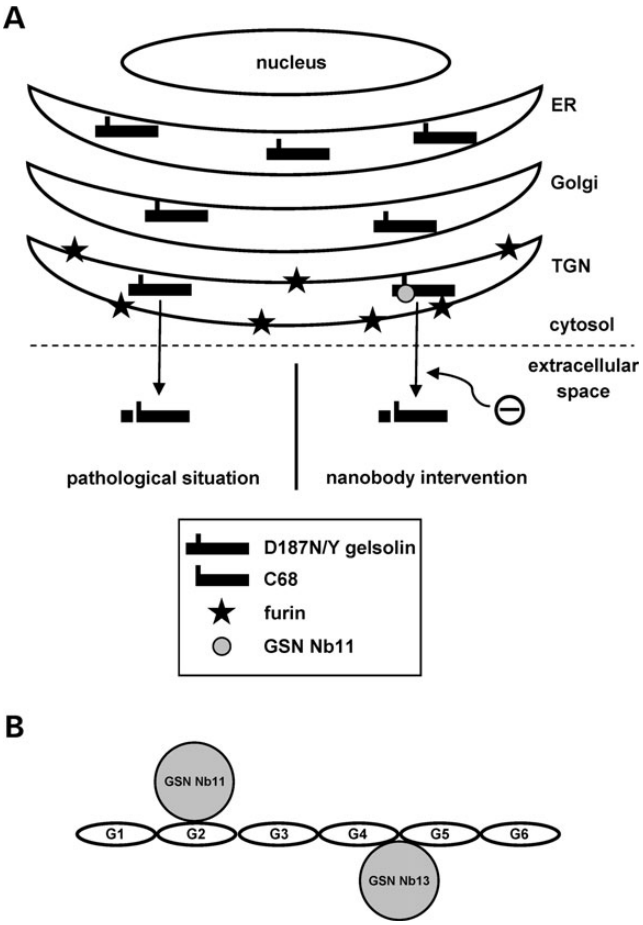

Figure 1 Secretory pathway of (mutant) plasma gelsolin and ER-directed GSN Nb11. (**A**) Mutant plasma gelsolin is directed to the endoplasmic reticulum (ER) where it is destined to follow the secretory pathway. Throughout its passage via the ER and Golgi network, maturation and packaging of secreted proteins occur before they are sent towards the plasma membrane. In the *trans*-Golgi network, mutant plasma gelsolin encounters furin, a membrane-associated proprotein convertase. The D187N/Y mutation makes mutant plasma gelsolin susceptible to furin proteolysis, which is not the case in the wild-type form. Upon furin proteolysis, a C-terminal 68 kDa fragment arises and is secreted in the extracellular space where it acts as precursor for a second aberrant proteolysis by MT1-MMP. The ER-directed GSN Nb11 used in this study, follows the same pathway as described and is meant to bind plasma gelsolin in order to protect it against furin proteolysis in the *trans*-Golgi network. (**B**) Schematic representation of GSN Nb11/13, bound to gelsolin. GSN Nb11 binds G2, GSN Nb13 binds G4-5.

confirmed by ELISA (Supplementary material, Fig. S3). We repeated the *in vitro* furin assay with His-tagged mutant gelsolin domain 2 (G2*) alone (^{132}G-^{286}S), instead of full-length plasma gelsolin (Fig. 2D). In the positive control sample (Fig. 2D, lane 2) in which G2* and furin were incubated, we observed 2 degradation fragments. Upon addition of GSN Nb11, the signal intensity of proteolyzed fragments was progressively reduced as the GSN Nb11 concentration was elevated. We conclude that furin does not require gelsolin domains other than G2* to be able to interact and perform cleavage of the full-length mutant plasma gelsolin and that GSN Nb11 reduces furin proteolysis of G2*.

GSN G2:Nb11 crystal structure provides insight in furin proteolysis reduction mechanism

To further gain insight into the mechanism by which C68 formation is reduced by GSN Nb11, we performed crystallography on the G2:Nb11 complex (Fig. 3). The crystal structure of the active conformation of calcium-bound domain 2 (^{159}V–^{259}D) of human gelsolin (G2) in complex to GSN Nb11 was determined at 2.6 Å resolution. The data collection and refinement statistics are detailed in Supplementary material, Table S1. Structural analysis revealed that Nb11 does not directly block the furin cleavage site at Ala-173 but binds the short α–helix of the G2 domain (Fig. 3A). Since GSN Nb11 binds G2 at a site distant to the Asp-187 residue, we do not expect the mutant G2:Nb11 interaction surface to be significantly different from what we observed in the G2:Nb11 crystal structure. In gelsolin domain 2 of the G2:Nb11 complex, the type-2 calcium-binding site is occupied, with the calcium ion coordinated by Asp-187, Glu-209 and Asp-259, and the disulfide bond between Cys-188 and Cys-201 is intact (Fig. 3B). These features are testament to the correct folding of G2 in the absence of the other five gelsolin domains. The G2 structure is highly similar to the corresponding domain in the human G1–G3/actin complex structure (PDB 3FFK) characterized by a root-mean-square deviation (RMSD) of 0.84 Å between the two G2 structures, indicating that Nb11 binding does not induce significant conformational changes in G2 (Fig. 3B). Structural comparison of the G2:Nb11 complex with unbound Nb11 showed that the mechanism of protection does not involve major conformational changes in Nb11 upon G2 binding (Supplementary material, Fig. S4). Superimposition of the bound and the unbound forms of Nb11 revealed an RMSD of 0.426 Å for 747 atoms. The positions of the G2-binding residues are highly conserved. Only ^{29}Phe relocates to create space for the tight G2:Nb11 interaction. When the GSN Nb11 crystal is evaluated upon interaction with

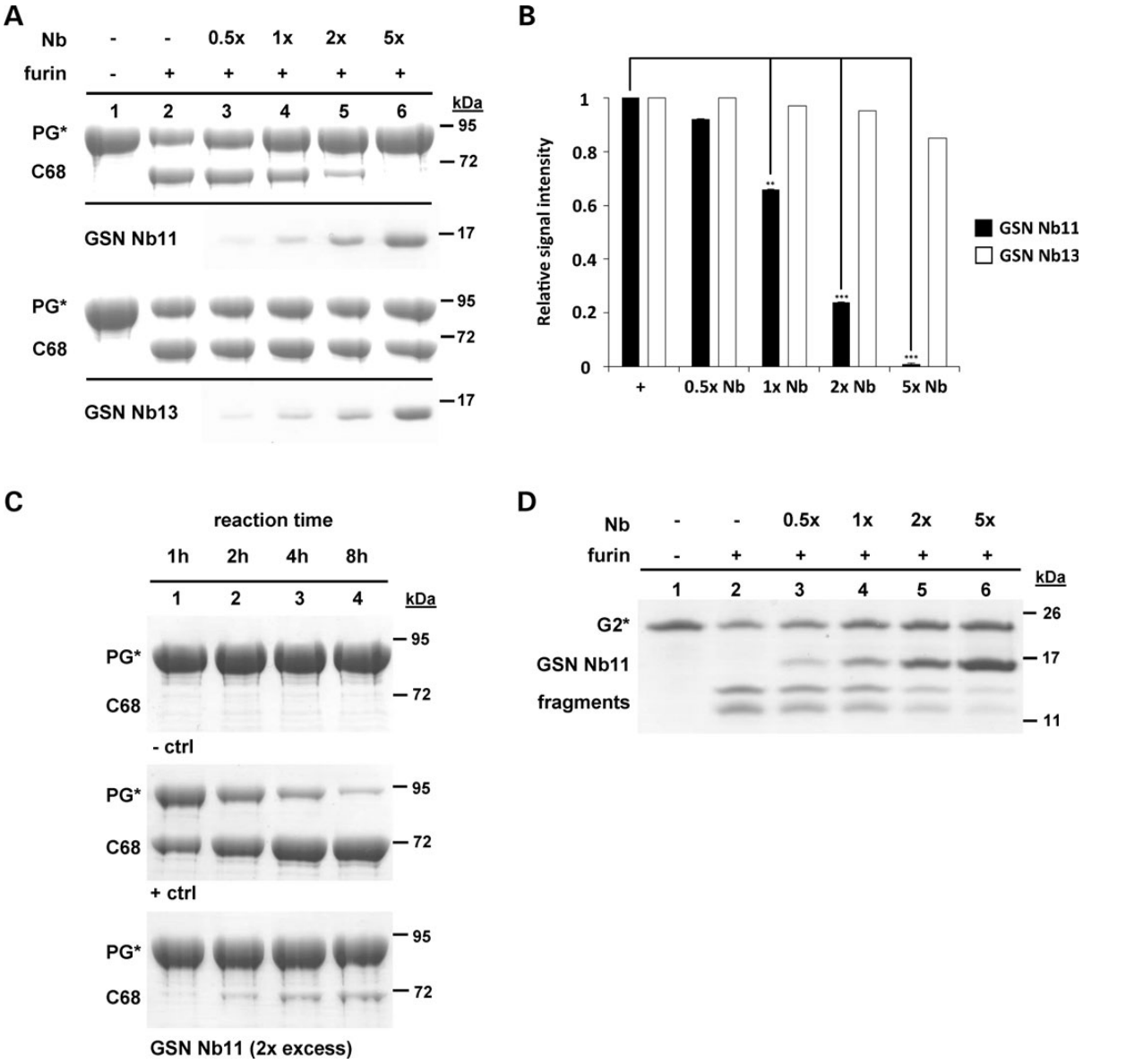

Figure 2 Gelsolin Nb11 specifically disturbs the plasma gelsolin–furin interaction *in vitro*. (**A**) *In vitro* furin cleavage assay in which 1 h incubation of furin with PG* generates C68. Pre-incubation of GSN Nb11 (upper panel) with PG* reduced the amount of C68 generated by furin proteolysis in a concentration dependent manner. Negative and positive controls were included (lanes 1 and 2, respectively). Molar ratio nanobody:PG* is indicated by ×0.5–×5 in lanes 3–6. GSN Nb13 (lower panel) that binds gelsolin domains 4–5, irrelevant to furin proteolysis, had no reducing effect on C68 formation (lanes 3–6). (**B**) Quantification of the *in vitro* furin assay, shown in A. Data are represented relative to the positive control. C68 signal intensity is reduced by 34% ($n = 3$, $P = 0.008$; ×1), 76% ($n = 3$, $P = 0.0003$; ×2) and 99% ($n = 3$, $P = 2\times10^{-5}$; ×5). Relative C68 signal intensity is shown as mean of triplicates + SE, $^{**}P < 0.01$; $^{***}P < 0.001$. (**C**) *In vitro* furin cleavage reaction using ×2 molar excess of GSN Nb11, with reaction times of 1, 2, 4 and 8 h (lanes 1–4). Negative (upper panel) and positive (middle panel) controls were included. GSN Nb11 upholds its effect at the various time points (lower panel, lanes 1–4). (**D**) *In vitro* furin cleavage assay with isolated mutant G2 domain. Furin is able to perform proteolysis on the isolated mutant G2 domain (lane 2). GSN Nb11 has the same effect on furin proteolysis as in A.

G1–G2–G3, we observe binding of GSN Nb11 to the short α-helix of G2 that is followed by the G2–G3 linker (which harbors Asp-259 that co-coordinates calcium) (Fig. 3C, shown in blue). Since we noted that Nb11 does not induce conformational changes in G2 (Fig. 3B), a change in conformation of the G2–G3 linker might be responsible for the protective effect towards the furin cleavage site (Fig. 3C, β-sheet bearing the Ala-173 cleavage site shown in pink). We hypothesized that GSN Nb11 binding is stabilizing the short α-helix of G2 and directing the subsequent chain to cover the furin cleavage site. To investigate this hypothesis, we performed a furin cleavage assay using a truncated G2* domain lacking the G2–G3 linker (Supplementary material, Fig. S5). This shortened G2* (with ^{259}D as C-terminal residue) was also protected from furin cleavage by GSN Nb11 so the G2–G3 linker is most likely not involved in the inhibitory process.

Analysis of the interacting surfaces between G2 and Nb11 reveals a variety of hydrogen bonds, salt bridges and hydrophobic interactions (Supplementary material, Table S2). The interface spans an area of 610 Å^2, which comprises 11 and 9% of the solvent accessible surfaces of G2 and Nb11, respectively. All of the Nb11 complementarity-determining regions (CDR) loops contribute hydrogen bonds to the interface with G2, while CDR1 and CDR3 also participate on hydrophobic interactions with G2, and CDR3 forms salt bridges with G2 (Supplementary material, Table S2 and Fig. S6).

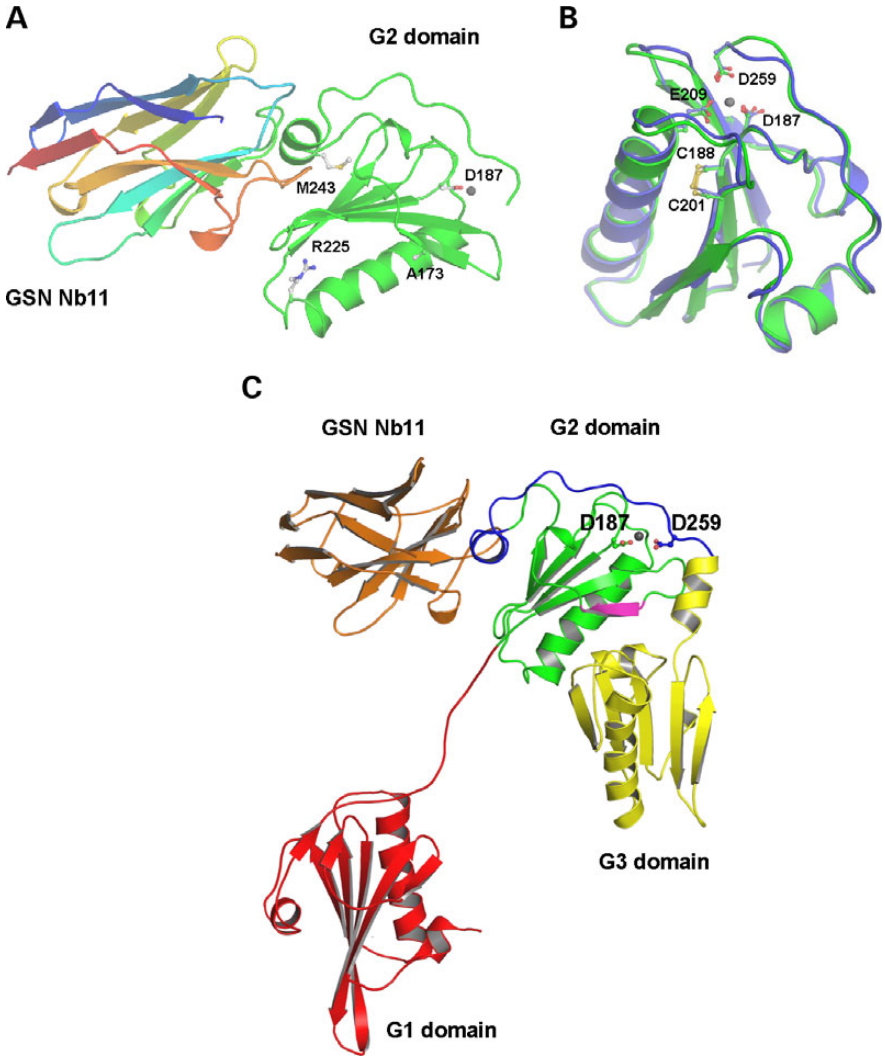

Figure 3 Gelsolin G2:Nb11 crystal structure. (**A**) GSN Nb11 binds G2 at a distant site relative to the furin cleavage site (A173). Calcium is shown as a dark grey sphere; D187 is the gelsolin amyloidosis mutation site. Furin cleavage site (A173) and MT1-MMP cleavage sites (R225 and M243) are shown in ball-and-stick representations. (**B**) Superposition of G2 (V159-D259) as determined in the G2-Nb11 structure and G2 derived from the N-terminal active gelsolin/actin complex (PDB: 3FFK). Ribbon representation shows G2 from G2-Nb11 in green and from 3FFK in blue. Cysteine residues forming a disulfide bond and the calcium binding site are presented as ball-and-stick with parental colors and calcium is in grey. (**C**) GSN G2:Nb11 was overlaid onto the active N-terminal half of gelsolin (PDB: 3FFK). The β-sheet harboring the furin cleavage site is shown in pink; the short α-helix and G2-G3 linker are shown in blue.

Modeling of GSN Nb11 with full-length gelsolin showed that the nanobody does not interfere with the other gelsolin domains (Supplementary material, Fig. S7). To elaborate on the potential influence that GSN Nb11 might have on actin severing activity in plasma, the G2:Nb11 crystal structure was superimposed on G2 in the human G1–G3:actin complex structure, PDB 3FFK (Supplementary material, Fig. S8A and B). Subsequently, the actin from this Nb11: G1-G3:actin model was further superimposed on an actin protomer in an F-actin cryo EM structure (PDB 3G37) (Supplementary material, Fig. S8C). These models of overlaid structures indicate that GSN Nb11 will sterically clash with actin, preventing G2 bound to GSN Nb11 from interacting with either G- or F-actin, suggesting an inhibitory influence on plasma gelsolin severing activity.

GSN Nb11 retains the ability to reduce furin proteolysis of PG* when directed to the *trans*-Golgi network of HEK293T cells

To verify our findings in a more complex environment, we further elaborated our hypothesis by testing the effect of GSN Nb11 in HEK293T cells. Since furin is active in the *trans*-Golgi network (30) and therefore inaccessible to the nanobodies, we directed GSN nanobodies to the secretory compartment where they can bind PG* prior to encountering furin. To this end, we cloned an ER-targeting sequence N-terminally to GSN Nb11/13 (Fig. 4A). At the C-terminus, a V5 tag was linked in order to allow visualization. After transient transfection in HEK293T cells, wild-type and mutant plasma gelsolin (Supplementary material, Fig. S9A) and GSN Nb11/13 (Supplementary material, Fig. S9B) were co-stained with golgin (a *trans*-Golgi network marker) to confirm their co-localization in the secretory compartment. Next, the ER-directed Nb11/13 were transiently transfected in HEK293T cells together with wild-type or mutant full-length plasma gelsolin (Fig. 4B). Epifluorescence microscopy revealed co-localization of GSN Nb11/13 with both gelsolin variants (Fig. 4B, merged images). To investigate if transient transfection of the ER-directed GSN Nb11 could establish the same effect on gelsolin degradation by furin as was shown *in vitro*, we analyzed the cell medium (Fig. 4C). In the medium, secreted proteins are detectable and

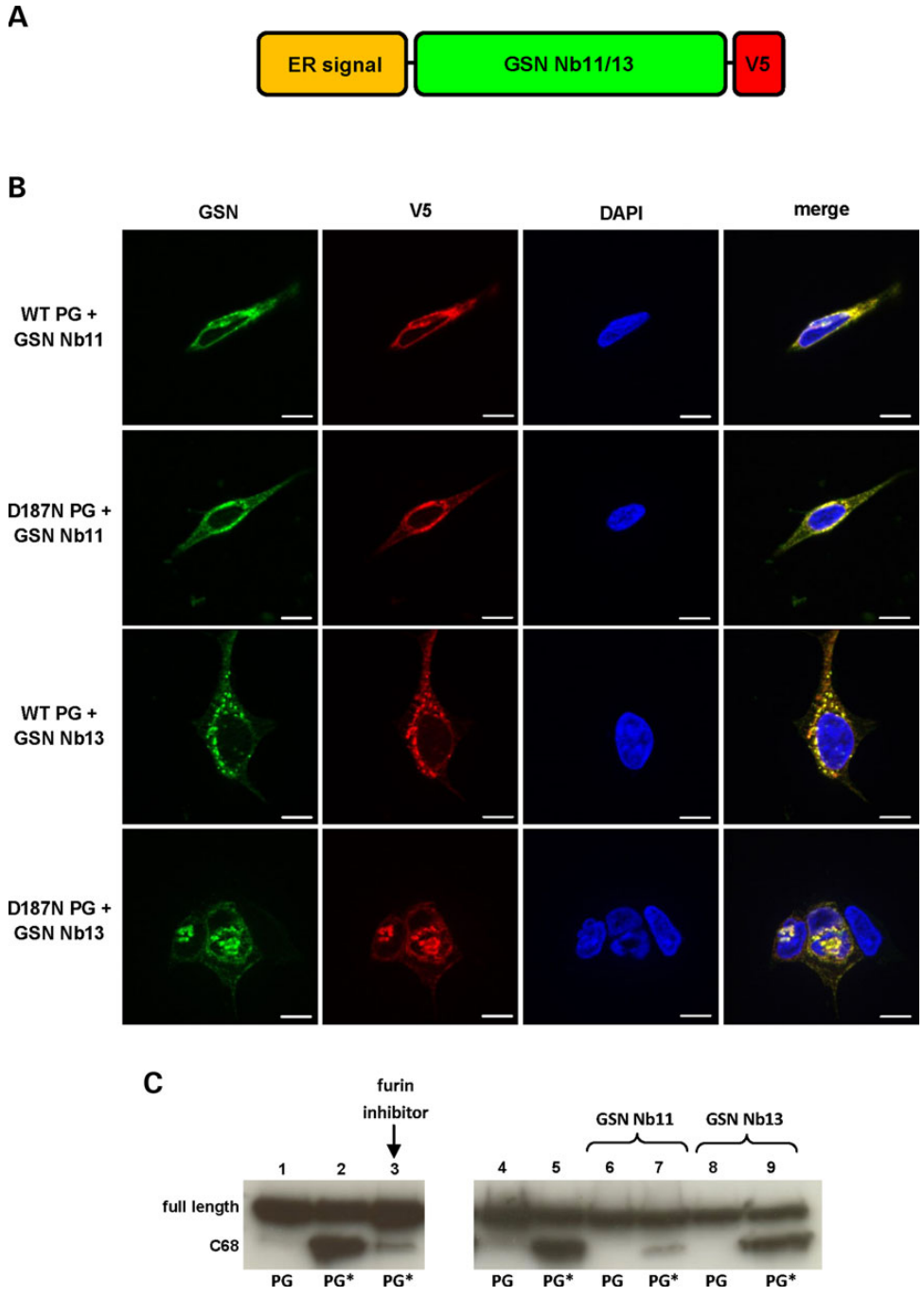

Figure 4 ER-directed gelsolin Nb11 reduces C68 secretion in HEK293T cells. Transient transfections of ER-directed GSN Nb11/13 and PG/PG* in HEK293T cells. (**A**) A GSN Nb11/13 construct (with N-terminal ER signal peptide) directs the GSN nanobodies to the secretory pathway of HEK293T cells. At the C-terminal end of the GSN nanobody, a V5-tag was cloned to allow visualization in immunocytochemistry and western blot analysis. (**B**) Wild-type (rows 1 + 3) and D187N (rows 2 + 4) plasma gelsolin (green) were co-transfected with ER-directed GSN Nb11 (rows 1–2) or GSN Nb13 (rows 3–4) (red) to validate co-localization in the secretory pathway in HEK293T cells (merged images). (Scale bar = 10 µm) (**C**) Western blot analysis of transfected HEK293T cell medium. Full length PG (left panel, lane 1), PG* and C68 (left panel, lane 2) are clearly detectable in the cell medium of transiently transfected cells. Addition of 100 µM furin inhibitor I in the cell medium results in defective furin activity and reduced C68 secretion (left panel, lane 3). Lanes 4–5 (right panel) show control signals for PG*/C68 secretion without GSN nanobody expression. Lanes 6 and 8 show wild-type PG secretion without proteolysis when co-transfected with GSN Nb11/13. The effect of GSN Nb11 and GSN Nb13 on C68 formation is detectable in lanes 7 and 9, respectively. GSN Nb11 strongly reduces C68 formation whereas GSN Nb13 has no influence (both in comparison to lane 5).

by probing for gelsolin by western blot analysis, we could monitor the PG* proteolysis level. As a positive control for furin inhibition, we used furin inhibitor I, a peptidyl chloromethylketone that binds irreversibly to the catalytic site of furin and blocks its activity. Post-transfection addition of 100 µM of this inhibitor drastically reduced C68 formation (Fig. 4C, left panel, compare lane 3 with lane 2). Co-transfection of PG* with ER-directed GSN Nb11/13 confirmed what we observed in the *in vitro* furin cleavage assay (Fig. 4C, right panel). Transfection of GSN Nb11 (Fig. 4C, right panel, lane 7) drastically reduced C68 formation, comparable to the effect of furin inhibitor I (Fig. 4C, left panel, lane 3). GSN Nb13 did not influence C68 formation (Fig. 4C, right panel,

lane 9). Wild-type gelsolin was not observed to be proteolyzed (Fig. 4C, right panel, lanes 4, 6, 8).

Development of a gelsolin nanobody secreting gelsolin amyloidosis mouse model

After verification of the GSN Nb11 effect in HEK293T cells, we wanted to further assess the therapeutic effect in an *in vivo* system. Transgenic gelsolin amyloidosis mice (28) express human mutant plasma gelsolin and the furin cleavage product C68 is found in the plasma of these mice. In order to direct gelsolin nanobodies to the murine secretory compartment, we developed mice expressing ER-directed GSN Nb11/13 for subsequent cross breeding with the gelsolin amyloidosis mice (Fig. 5). GSN amyloidosis/nanobody double-positive mice will express both transgenic proteins and in this manner, GSN Nb11/13 will encounter PG* in the secretory compartment. ER-directed GSN Nb11/13 cDNA was cloned in the pROSA-DV2 vector, a vector targeting the ROSA26 locus (Fig. 5A). Insertion at this particular gene locus was meant to result in constitutive, ubiquitous expression of gelsolin nanobodies. After electroporation of the targeting vector in G4 ES cells, we checked for positive clones by Southern blotting (Fig. 5B). Positive colonies were transfected with the cre-recombinase and mRNA was isolated from these cells to check for nanobody presence at the RNA level (Fig. 5C). Nanobody positive ES cells were aggregated with Swiss inner cell mass (ICM) cells and the resulting blastocysts were transferred to the uteri of pseudopregnant Swiss fosters which resulted in a chimeric offspring (Fig. 5D). This offspring were backcrossed with wild-type C57BL/6 to check for germline transmission (Fig. 5E). Pups with nanobody cDNA in the germline cells were crossed with Cre deleter mice to remove the floxed STOP-cassette and activate transcription of the nanobody cDNA (Fig. 5F). Offspring were genotyped for nanobody and Cre and Nb/Cre double positive pups were checked for nanobody presence in the plasma by co-immunoprecipitation and western blot analysis (Fig. 5G). In a final step, these nanobody mice were crossed with gelsolin amyloidosis homozygotes to create GSN amyloidosis/nanobody double-positive mice. As a final verification, the offspring were genotyped for gelsolin amyloidosis and checked for nanobody expression in the plasma (Fig. 5H).

GSN Nb11/13 specifically bind human gelsolin in the GSN amyloidosis/nanobody mouse

Plasma was evaluated by western blot analysis and co-immunoprecipitation to estimate expression levels of transgenic human PG* and gelsolin nanobody in the double-positive mice (Fig. 6A and B). Approximate values of 200 and 100 ng protein per milligram plasma (PG* and Nb, respectively) result in plasma concentrations of ~10 and 5 µg/ml, respectively. For the conversion of concentration per mass to per volume, we used a reference value of 50 mg of total protein per milliliter of blood (31). The GSN amyloidosis/nanobody transgenic mice also express endogenous mouse plasma gelsolin, apart from the transgenic human PG* form. For this reason, it was important to verify to what extent the gelsolin nanobodies would cross-react with mouse gelsolin, once expressed in the transgenic nanobody mice. We performed co-immunoprecipitation experiments on mouse plasma, taken from wild-type mice and gelsolin amyloidosis homozygote mice (Fig. 6C). In albumin-cleared plasma from wild-type mice (Fig. 6C, upper panels), endogenous gelsolin was detected with a polyclonal gelsolin antibody (Fig. 6C, upper panels, lane 1). Non-specific interaction of endogenous plasma gelsolin with the V5 agarose was absent (Fig. 6C, upper panels, lane 2). Neither excess recombinant GSN Nb11 nor GSN Nb13 co-immunoprecipitated mouse plasma gelsolin (Fig. 6C, upper panels, lanes 3 and 4, respectively). As a positive control in this experiment, a similar co-immunoprecipitation experiment was performed on plasma from 4-months-old homozygous gelsolin amyloidosis mice (Fig. 6C, lower panels). Using the anti-FAF antibody, we can specifically detect human full length and C68 gelsolin formats in the albumin cleared plasma (Fig. 6C, lower panels, lane 1). Non-specific interaction with the V5 agarose was not observed (Fig. 6C, lower panels, lane 2) but we observed co-immunoprecipitation between human gelsolin formats for both recombinant GSN Nb11 and GSN Nb13 (Fig. 6C, lower panels, lanes 3 and 4). It is clear that the binding tendency of GSN Nb13 to the C68 fragment is much higher when compared with GSN Nb11. This can be explained by the fact that the epitope of GSN Nb11 resides in domain 2, which is truncated in C68. The epitope of GSN Nb13 is in gelsolin domains 4–5 which is unaffected in C68 and thus still accessible. These experiments show that 'dilution' of the potential therapeutic effect by cross reaction of GSN Nb11 with endogenous mouse plasma gelsolin is expected to be minimal.

GSN Nb11 expression in gelsolin amyloidosis mice positively affects transgenic mutant gelsolin proteostasis in skeletal muscle tissue

We evaluated the effect of GSN Nb11/13 expression in gelsolin amyloidosis mice by analysis of muscle tissue at different time points in the different groups. FAF Nb1, a previously characterized nanobody, was used as primary antibody in immunohistochemistry analysis (22). This nanobody was shown to bind all gelsolin formats, with a preference for the 8 kDa peptide and C68 fragment. Analysis of the heart muscle confirmed the staining specificity since in the 3-month-old mice, no (background) staining was observed (Supplementary material, Fig. S10A). In every group (control, Nb11 and Nb13), the staining becomes perceptible at the age of 6 months (Supplementary material, Fig. S10B) and persists at 9 months (Supplementary material, Fig. S10C). Since the staining pattern in the heart tissue was not homogeneous around the slide, no quantification of gelsolin staining was performed on the heart tissue and no effect of nanobody expression was evaluated. In contrast to the cardiac tissue, gelsolin staining was present in the musculus gastrocnemius at the ages of 3, 6 and 9 months (Fig. 7A–C). Costaining for laminin was performed to rule out artifacts and to make sure intact muscle tissue was evaluated. Gelsolin staining was homogeneous around the tissue slide and quantification of gelsolin staining surface was performed for every group at the ages of 3, 6 and 9 months (Supplementary material, Fig. S11). Gelsolin staining in 3-month-old mice was reduced with 27 ± 9% ($P < 0.05$) in GSN Nb11 expressing mice compared with littermate controls. Staining reduction in comparison to GSN Nb13 mice was 32 ± 8% ($P < 0.05$) (Supplementary material, Fig. S11A). In 6-month-old mice, no statistical relevant differences were observed (Supplementary material, Fig. S11B). When the mice reached the age of 9 months, a gelsolin staining reduction was discerned between GSN Nb11 mice and littermate controls (28 ± 9%, $P < 0.05$) (Supplementary material, Fig. S11C).

Reduction of aberrant furin proteolyis by GSN Nb11 results in improved muscle contractile properties

To test if the altered gelsolin staining patterns had an influence on muscle functionality, we examined muscle contractile

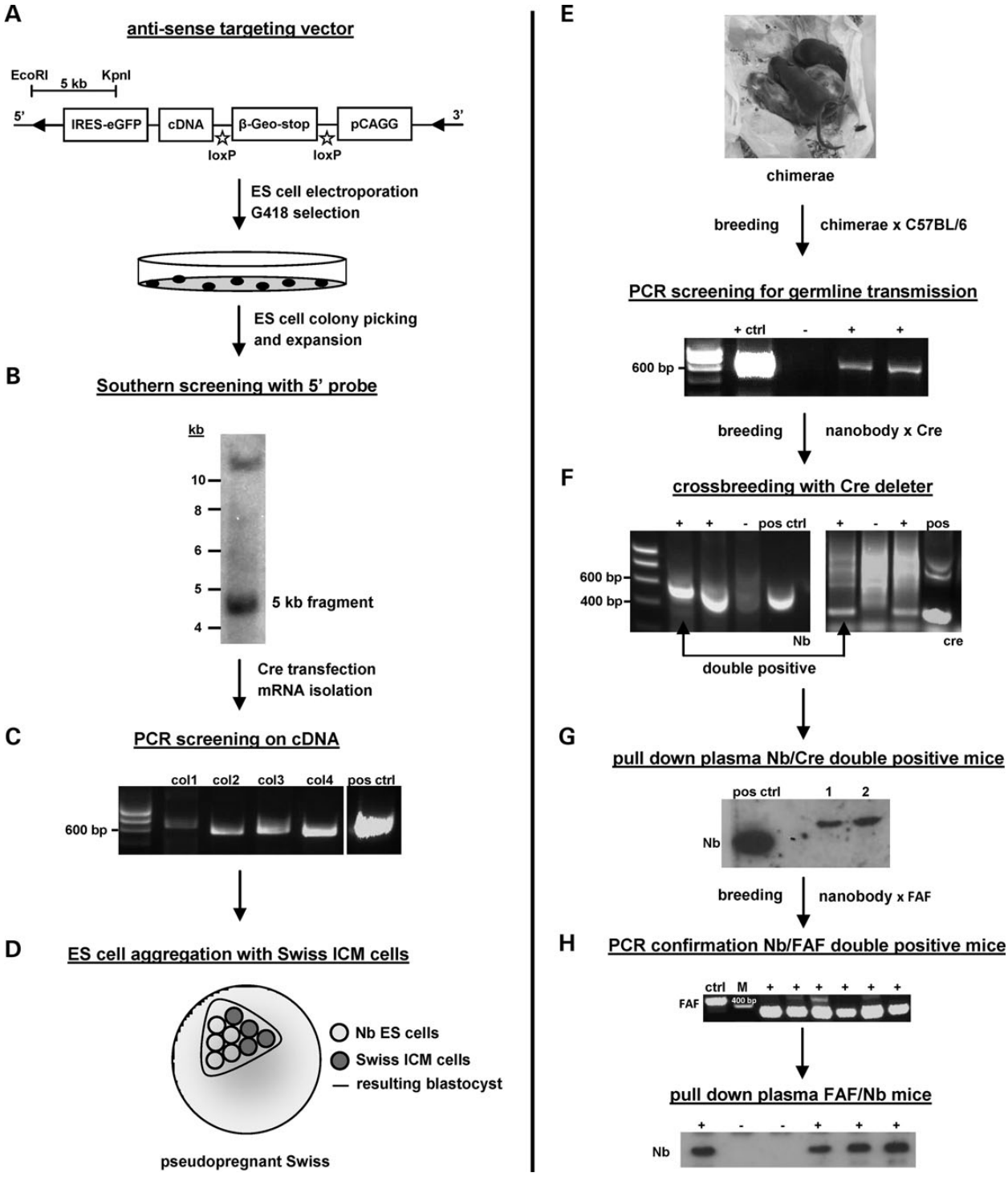

Figure 5 Development of transgenic, GSN Nb11/13 expressing gelsolin amyloidosis mice. (**A**) A pROSA26-DV2 targeting vector containing the ER-directed GSN Nb11/13 was developed to insert the GSN nanobodies in the murine genome at the ROSA26 locus. The anti-sense targeting vector was linearized and electroporated in G4 ES cells. The electroporated ES cells underwent G418 selection and after 7–10 days, surviving colonies were picked and expanded. (**B**) Successful integration in the ES cell genome was confirmed by Southern screening. A radioactive probe was used to detect a 5 kb fragment at the 5′ end in positive colonies. These positive colonies were grown again, the Cre plasmid was transfected to drive transcription and mRNA was isolated to make cDNA. (**C**) This cDNA was used a template for a PCR analysis using nanobody specific primers. (**D**) Following this extra verification step, positive ES cell clones were aggregated with Swiss ICM cells to form a blastocyst overnight. The resulting blastocyst was transferred to the uterus of a pseudo pregnant Swiss female. From the blastocyst, chimeric offspring was born. (**E**) These chimerae were bred with wild-type C57BL/6 mice to check for germline transmission in the offspring (by PCR screening of extracted DNA from the tail). At this stage, mice were available with successful insertion of the ER-GSN Nb11/13 transgene. However, in these mice, the STOP-cassette was still present between promotor and cDNA (floxed between loxP sites). (**F**) To remove the STOP-cassette, the mice were crossed with Cre deleter mice. (**G**) Offspring from this breeding were checked for GSN Nb11/13 expression at the protein level by means of immunoprecipation from plasma and western blot analysis. (**H**) Mice that were positive at this stage were finally crossed with homozygous FAF mice in order to obtain offspring that secrete both mutant plasma gelsolin and ER-directed nanobody.

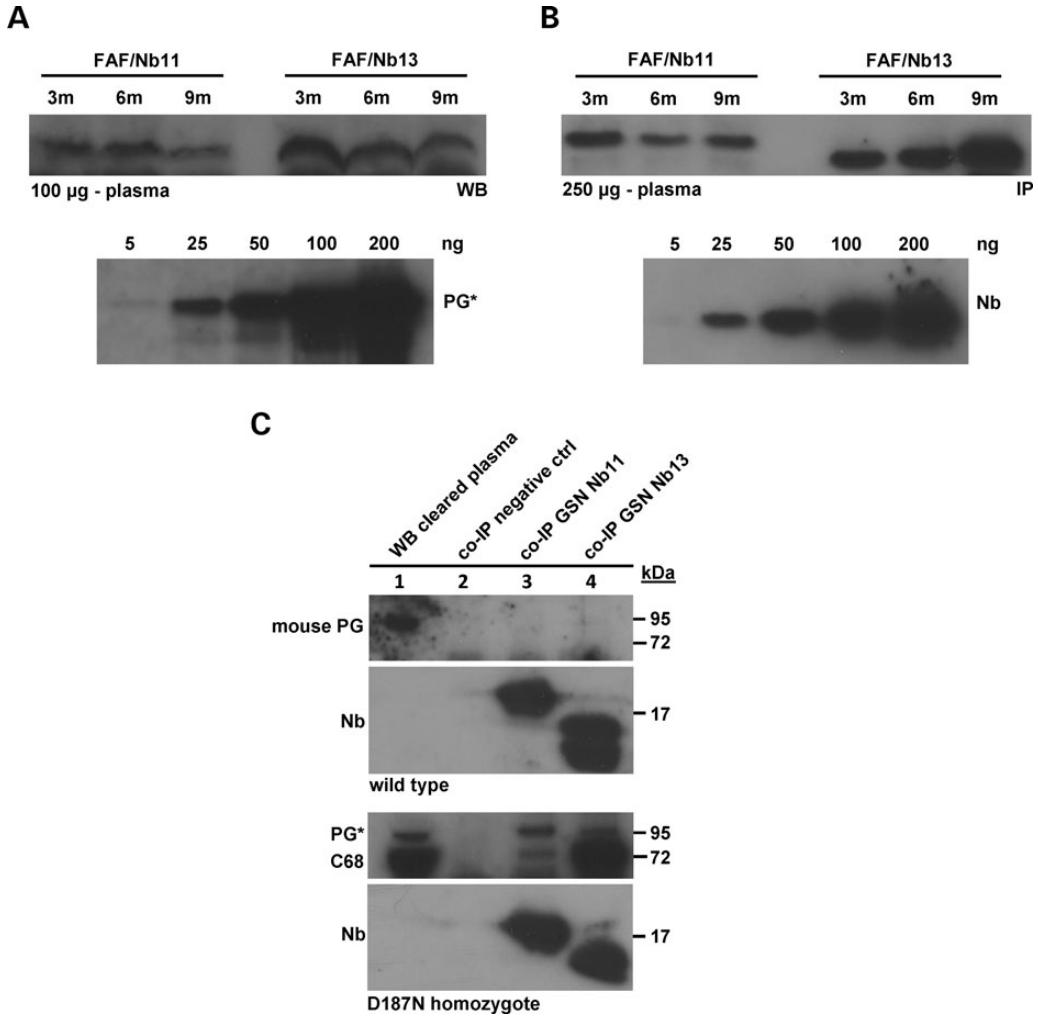

Figure 6 Quantification of expression levels in blood and cross-reactivity assessment of Nbs. (**A**) PG* expression estimation through western blot analysis of FAF/nanobody mice plasma. 100 µg of plasma (upper panel) and a concentration series of recombinant PG* (lower panel) were fractionated by SDS–PAGE and analyzed by western blot analysis. 100 µg of plasma contained ∼20 ng of PG*, this correlates with a concentration of 10 µg/ml of plasma. (**B**) Nanobody expression estimation through co-immunoprecipitation of FAF/nanobody mice plasma. 250 µg of plasma was incubated with V5-agarose and bound protein was evaluated by SDS–PAGE and western blot analysis (upper panel). In the lower panel, a concentration series is shown. 250 µg of plasma contained ∼25 ng of nanobody, which correlates with a concentration of 5 µg/ml. (**C**) Upper panels: co-immunoprecipitation on plasma from wild-type animals; mouse plasma gelsolin is detected in albumin cleared plasma with polyclonal gelsolin antibody (lane 1). Mouse plasma gelsolin displays no non-specific interaction with V5 agarose (lane 2) and was not co-immunoprecipitated by GSN Nb11 (lane 3) or GSN Nb13 (lane 4). Lower panels: co-immunoprecipitation on plasma obtained from homozygous gelsolin amyloidosis mice. PG* and C68 are detected in albumin cleared plasma with anti-FAF antibody (lane 1). Neither PG* nor C68 display non-specific interaction with V5 agarose (lane 2) and both gelsolin formats were co-immunoprecipitated by GSN Nb11 (lane 3) and GSN Nb13 (lane 4).

properties of the transgenic mice. GSN Nb13 expressing mice showed no differences in staining pattern when compared with littermate controls and this group was consequently not included in the experiment (as were mice of 3- and 6-month old). *In vitro* contractile functions were investigated in two different hind-leg muscles: extensor digitorum longus (EDL) and soleus. Intact incubated muscles were electrically stimulated repeatedly to evoke tetanic contractions. Typical features of a fatiguing protocol are a decrease in force development and reductions of contraction and relaxation speed. The decrease in contraction speed was strongly attenuated, across the entire 8-min fatigue protocol, in EDL, but not in soleus of the GSN Nb11 mice compared with littermate controls (Fig. 8A and B). Neither the decrease in force development nor the relaxation speed was affected by the intervention in EDL and soleus (Supplementary material, Fig. S12). However, the force development (expressed relative to maximal force) in resting state was higher in the GSN Nb11 mice at a frequency of 20 Hz in soleus, but not significantly at other frequencies, nor in EDL (Fig. 8C and D), suggesting that the calcium handling during single muscle contractions was slightly improved by the intervention.

Discussion

Correct folding is essential for proteins to execute their function. Complex systems have evolved to assist folding, prevent aberrant folding and clear misfolded proteins. A myriad of quality control (QC) systems prevents disturbed proteostasis (32) but in certain cases, these QC systems are overloaded or defected and they fail to ensure proper transcription, translation and secretion of proteins. Amyloid disease develops when misfolded proteins aggregate and form (pre-)fibrillar structures that are toxic to the affected tissue. A lot of research effort has been put in targeting toxic oligomeric intermediates (33), amyloid fibril formation (34)

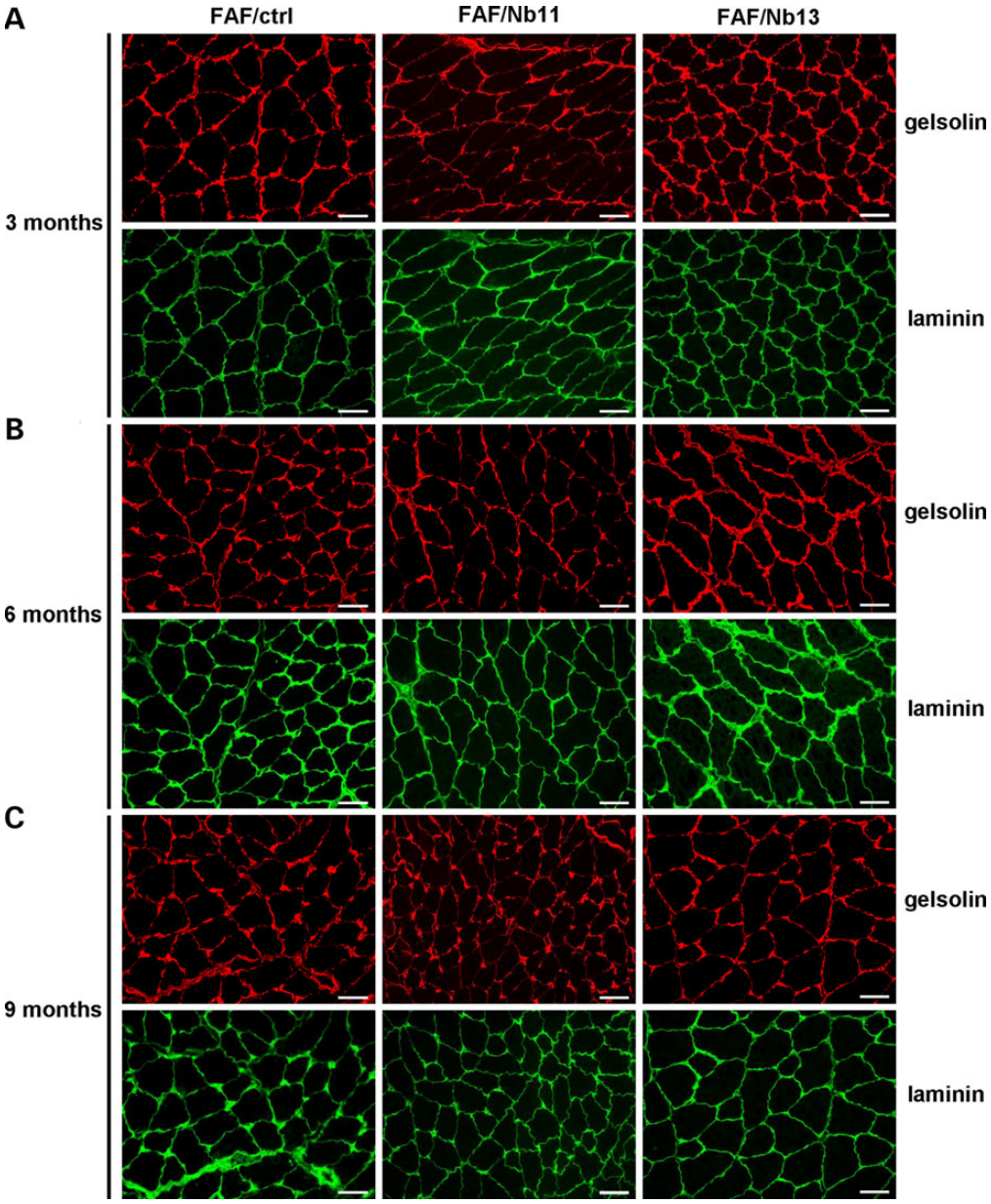

Figure 7 Immunohistochemistry analysis in musculus gastrocnemius of gelsolin amyloidosis mice at the age of 3, 6 and 9 months. Musculus gastrocnemius tissue was dissected from gelsolin amyloidosis mice expressing GSN Nb11/13 and their nanobody negative littermate controls. Immunohistochemistry staining was done for gelsolin (red) and laminin (green) on mice of 3, 6 and 9 months old (**A**, **B** and **C**, respectively) (scale bar = 50 µm).

or even extracellular matrix components (35). These therapeutic approaches try to intervene with stages following the genesis of amyloidogenic peptides. In this study, we aimed to interfere with the pathological proteolytic cascade of the disease, prior to amyloid peptide formation. Recently, we have shown that C68 binding nanobodies are able to reduce proteolysis by MT1-MMP-like proteases in the gelsolin amyloidosis mouse model (22).

In the present study, we targeted the protease that initiates the whole pathological process: furin. This proprotein convertase is an essential, ubiquitously expressed protease (36) and hence not a suitable candidate for direct therapeutical targeting. However, we influenced furin activity indirectly by aiming for its substrate: mutant plasma gelsolin. Gelsolin nanobodies are proved to have an impact on proteolysis by contaminating *E. coli* proteases in recombinant gelsolin samples (18). Some nanobodies accelerated the proteolytic breakdown of gelsolin, yet others slowed down the proteolysis. Thus, the nanobody–gelsolin interaction can protect gelsolin from proteolytic processing.

In a similar fashion, we wanted to use GSN Nb11 as armor to protect mutant plasma gelsolin from pathological furin proteolysis. *In vitro* assays and HEK293T cell studies confirmed our hypothesis and showed a reducing effect of GSN Nb11 on furin proteolysis. Structural analysis of the gelsolin G2:GSN Nb11 complex revealed that Nb11 does not directly block the cleavage site at ^{172}Arg–^{173}Ala. Superposition of G2 from the G2:Nb11 complex and the N-terminal active gelsolin:actin complex suggested that GSN Nb11 does not induce a major conformational change in the G2 domain. We also found that the inhibitory effect does not involve major structural changes in GSN Nb11 nor stabilization of the G2–G3 linker to cover the furin cleavage site. This

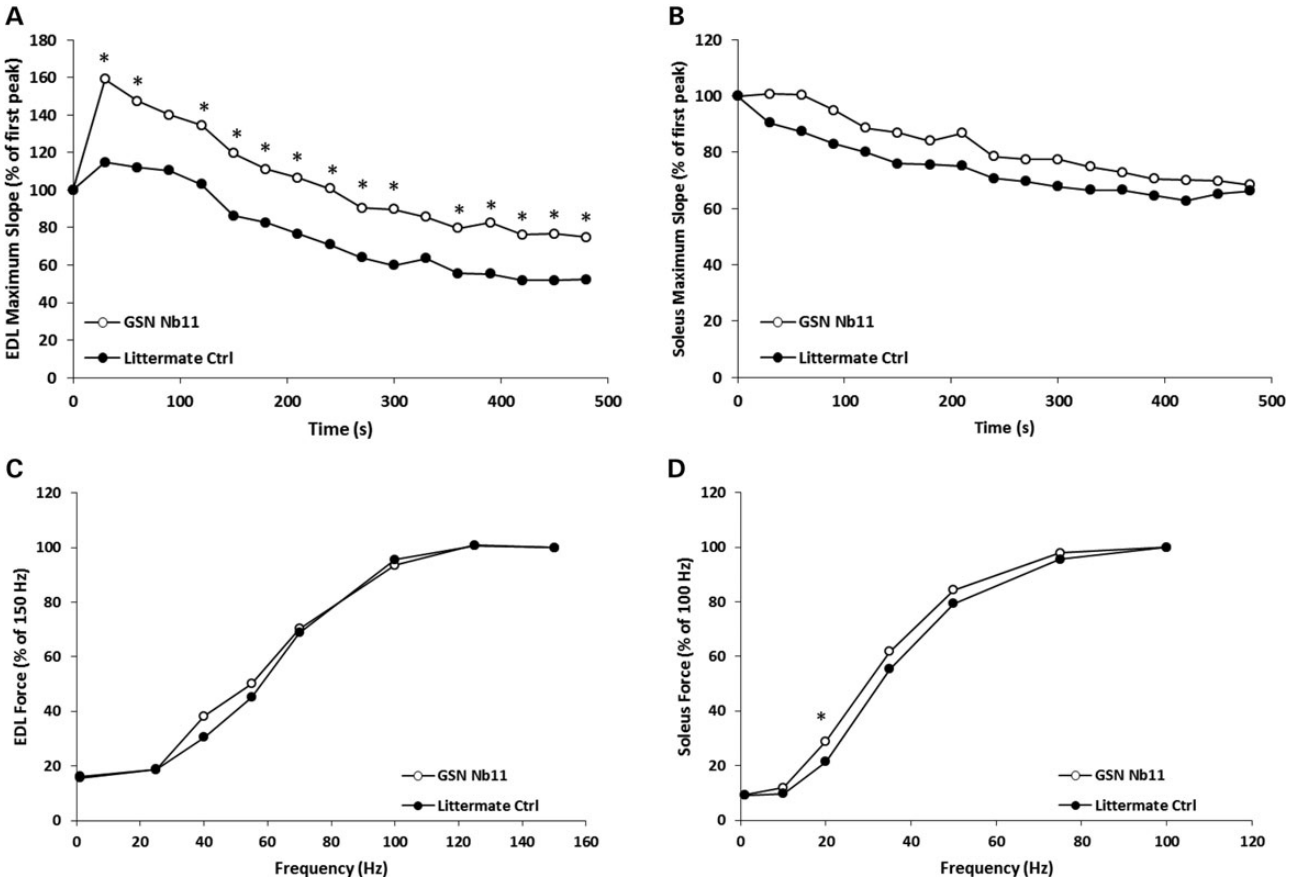

Figure 8 Muscle contractile properties of gelsolin Nb11 expressing heterozygotes and their littermate controls. Repeated *in vitro* muscle contractions in GSN Nb11 gelsolin amyloidosis mice (white dots) compared with littermate controls (black dots). (**A** and **B**) GSN Nb11 expression resulted in an attenuation of the slowing of contraction speed during fatigue in EDL (A), but not in soleus (B), * $P < 0.05$ GSN Nb11 ($n = 5$) versus littermate controls ($n = 5$). (**C** and **D**) No significant between-group differences were detected in force–frequency relationship in EDL (expressed relative to maximal force)(C). In soleus (D), relative forces were higher at 20 Hz ($P = 0.002$) in GSN Nb11 ($n = 5$) compared with littermate controls ($n = 5$) (* $P < 0.05$; two sided unpaired *t*-test).

leaves two possibilities as to the mechanism of protection. The first possibility is that Nb11 binding may hinder the cleavage site from reaching to the binding pocket of furin by interaction with a distant site on G2*. The second possible mechanism of protection is that the Nb11 interaction specifically stabilizes the inactive or active conformations of gelsolin G2 in the FAF mutant, since in both conformations the cleavage site is protected from furin cleavage (10). Unlike the MT1-MMP-like proteases that were targeted in our previous study (22), furin is an intracellular protein, active in the *trans*-Golgi network (TGN) and shuttling to the plasma membrane (30). This made it impossible to inject GSN Nb11 in gelsolin amyloidosis mice since the nanobody cannot permeate several membrane barriers to reach the TGN. For that reason, we designed a transgenic mouse expressing ER-directed GSN Nb11. Secreted Nb11 will pass the TGN while traversing the secretion pathway and encounter mutant plasma gelsolin. This is the first study reporting a mouse that expresses a therapeutic nanobody, demonstrating the versatility of the nanobody technology.

Expression of a gelsolin nanobody in mice had potential consequences in terms of cross-reactivity. Apart from the mutant human plasma gelsolin, the endogenous mouse plasma gelsolin is also expressed in the gelsolin amyloidosis mice. We have demonstrated that interaction of the gelsolin nanobodies with the endogenous gelsolin is unlikely so cross-reaction effects in mice are improbable. In a previous study, AST/ALT (aspartate transaminase/alanine transaminase) measurements in nanobody injected mice indicated that nanobody presence in plasma does not trigger adverse effects (22). Extrapolation of the intracellular shielding approach to human patients would imply gene therapy. The last two decades, new strategies concerning targeted gene transfer are investigated thoroughly, both viral (37,38) as well as non-viral approaches (39). Effective targeting of GSN Nb11 to specific organs might result in a therapeutic merit for the affected patients.

Severing experiments with plasma of gelsolin amyloidosis patients showed that mutant plasma gelsolin loses severing activity (40). Homozygous patients lose all activity, and heterozygous patients retain 50% activity because they still have a wild-type allele. Yet, the actin scavenging system in plasma of gelsolin amyloidosis patients is not affected in a problematic way (41). Other actin-binding proteins such as vitamin D binding protein (DBP, present in high concentrations) act redundantly by sequestering G-actin monomers (42). For this reason, radical side effects on actin scavenging capacity of wild-type plasma gelsolin are not expected to be induced by GSN Nb11 when blocking the interaction with monomeric and filamentous actin. In addition, it is important to note that the expression level of transgenic nanobody in our mouse model was estimated by measuring the amount of free nanobody in the plasma. Since the nanobody is ubiquitously expressed, we have to be aware of the fact that only a fraction of secreted nanobody originates from muscle

tissue, also expressing mutant plasma gelsolin. However, in our mouse model, the relatively low expression level was sufficient to establish a therapeutic effect. *In vitro* furin cleavage assays showed that the reducing effect of GSN Nb11 on C68 formation was amplified when using increasing concentrations of GSN Nb11 versus mutant PG. Hence, when applied to human patients, the GSN Nb11 dose will be a determining factor in establishing the therapeutic effect.

Translation of this approach into human patients using state-of-the-art gene transfer technology (43,44) would imply that the GSN Nb11 expression can be targeted in a more tissue-specific manner. Hence, the expression level would be more manageable, resulting in a greater therapeutic effect. In this study, we present a unique nanobody expressing mouse model that provides insights regarding novel strategies to counter amyloid diseases.

Materials and Methods

Antibodies and reagents

Monoclonal and polyclonal anti-V5 antibody was purchased from Life Technologies (Merelbeke, Belgium) (both 1:500 in ICC, 1:800 in IHC). Alexa Fluor 594 goat anti-rabbit IgG (H + L) antibody and 488 goat anti-mouse (H + L) were purchased from Invitrogen (Merelbeke, Belgium)(both 1:500 in IHC). Polyclonal anti-gelsolin antibody (1:100 in ICC) was obtained as described previously (45). Monoclonal anti-gelsolin (1:2000 in WB) was purchased from Sigma-Aldrich (Diegem, Belgium). Polyclonal golgin 245 (C-13) (1:200 in ICC) was obtained from Santa Cruz Biotechnology (Dallas, TX, USA). Polyclonal anti-FAF antibody (1:2000 in WB), raised against GST-tagged 8 kDa amyloidogenic peptide, was kindly provided by Dr Jeffery Kelly (Scripps Institute, CA, USA). Monoclonal anti-laminin antibody (1:500 in IHC) was purchased from Abcam (Cambridge, UK). Penta-His_6 horse radish peroxidase (HRP) coupled antibody was obtained from Qiagen (Venlo, The Netherlands). FAF Nb1-V5 was used as primary antibody in immunohistochemistry (22). Furin inhibitor I was purchased from Calbiochem (San Diego, CA, USA).

Recombinant protein purification

Performed as described previously (22).

cDNA cloning

Cloning of PG* in the pTrcHis-TOPO vector (Life Technologies, Merelbeke, Belgium) was performed using following primers: 5′ GCCACTGCGTCGCGGGGGGCG 3′ (forward) and 5′ GGATATCT GCAGAATTGCCCTAGGCAGCCAGCTCAGCCATGGC 3′ (reverse). PG was subcloned in the peGFP.N1 vector (Clontech, Mountain View, CA, USA) using HindIII and SacII. Quikchange site-directed mutagenesis was performed to introduce the D187N mutation in PG using following primers: 5′ GCCATGGCTGAGCTGGCTGCC TAGGGCAATTCTGCAGATATCC 3′ (forward) and 5′ GGATATCTG CAGAATTGCCCTAGGCAGCCAGCTCAGCCATGGC 3′ (reverse). GSN Nb11 and GSN Nb13 were cloned in the pCMV/myc/ER vector (Life Technologies, Merelbeke, Belgium) using 5′ GGC GGC GCG CAC TCC CAG GTG CAG CTG CAG GAG TCT GGA GG 3′ (forward) and 5′ CCCCTCGAGCGTAGAATCGAGACCGAGGAGAGGGTT AGG GATAGGCTTACCACCACCAGAACCACCACCACCGCTGGAGACGGT GACCTGGGTCCC 3′ (reverse). This reverse primer introduced a V5-tag between the inserted GSN nanobody and the myc-tag in the vector. A Quikchange site-directed mutagenesis kit (Stratagene, Santa Clara, CA, USA) was used to introduce a stop codon between the myc-tag and the KDEL retention signal. Following primers were used: 5′ GAGGATCTGAATGGGGCCGCATAAGAG AAGGACGAGCTGTAGTC 3′ (forward) and 5′ GACTACAGCTCGTC CTTCTCTTATGCGGCCCCATTCAGATCCTC 3′ (reverse). The ER-directed GSN Nb11/13 was subcloned from the pCMV/myc/ER vector to the pDONR207 vector (BCCM/LMBP) by means of the BP clonase II kit (Life Technologies, Merelbeke, Belgium) in order to generate an entry vector. AttB sites were included in both forward and reverse primer and the PCR product was used in a homologous recombinant reaction with the attP sites in pDONR207. Primers involved in the BP cloning reaction were 5′ GGGGACAAGTTTGTACAAAAAAGCAGGCTTCGCCACCATGGGATG GAGCTGT 3′ (forward) and 5′ GGGGACCACTTTGTACAAGAAAGCT GGGTCCTATGCGGCCCCATTCAGATC 3′ (reverse). 100 ng of the resulting entry vector, containing the GSN Nb11/13 cDNA was combined with 100 ng of pEntry L4-Caggs-loxpNeopolyaloxpR1, 100 ng of pEntry R2 IRES eGFP luciferase pA L3 and 2 µl LR clonase II mix (Life Technologies, Merelbeke, Belgium). TE buffer (pH 8.0) was added until a volume of 10 µl. This reaction mixture was incubated for 8 h at 25°C. Subsequently, 150 ng of pROSA-DV2 (anti-sense) and 1 µl of additional LR clonase II mix was added to the reaction mixture and incubated overnight at 25°C to create the final targeting vector. The reaction mixture was transformed in DH5α cells according to the manufacturer's instructions and incubated overnight on LB-agar plates containing 100 µg/ml ampicillin. Plasmid was purified from resulting colonies and checked by HindIII control digestion and DNA sequencing. The used constructs from the LR reaction were described previously (46).

In vitro furin assay

The *in vitro* cleavage reaction (47) was performed in a total volume of 20 µl. 3 µM purified recombinant PG* was incubated with GSN Nb11 (or negative control GSN Nb13) in reaction buffer (100 mM MOPS (3-(N-morpholino) propanesulfonic acid) pH 6.2, 2 mM $CaCl_2$, 1 mM DTT) for 1 h at 4°C. To initiate cleavage, 0.5 units of furin were added and the mixture was further incubated at 37°C for 1 h. The reaction was terminated by adding 5 µl Laemmli sample buffer and samples were immediately boiled for 5 min and analyzed by 10% SDS–PAGE and Coomassie staining. The C68 signal was quantified by using the Image J software. In the *in vitro* furin assay using the G2* domain lacking the G2–G3 linker (^{259}D as C-terminal residue), polyclonal anti-FAF antibody and penta-His_6 horse radish peroxidase (HRP) coupled antibody were used to detect G2* and GSN Nb11, respectively.

In vitro MT1-MMP assay

Performed as described previously (22).

HEK293T cell culture, transfections and microscopy

HEK293T cells were maintained at 37°C in a humidified 10% CO_2 incubator and grown in DMEM medium (Gibco Life Technologies, Grand Island, NY, USA) supplemented with 10% fetal bovine serum (Thermo Scientific, Erembodegem, Belgium). Transient transfection was performed using the $CaPO_4$ protocol. Coverslips were blocked with 1% bovine serum albumin and incubated with primary antibody for 1 h at 37°C. Next, the appropriate Alexa Fluor-conjugated secondary antibody was incubated at room temperature for 30 min. Nuclei were stained with DAPI (0.4 µg/ml) (Sigma, St Louis, MO, USA). Cells were mounted with VectaShield and imaged at room temperature using a Carl Zeiss Axiovert 200 M Apotome epifluorescence microscope equipped with a cooled CCD

Axiocam camera (Zeiss ×63 1.4NA Oil Plan-Apochromat objective) and Axiovision 4.5 software.

Cell lysate and medium analysis

Transiently transfected HEK293T cells were washed with PBS and disrupted in ice-cold lysis buffer (PBS + 1% Triton X-100, 1 mM PMSF and 200 µg/ml protease inhibitor cocktail). The extract was centrifuged (29 000*g*) for 10 min at 4°C, and the supernatant was collected. HEK293T cell medium was collected from the culture flask and centrifuged (29 000*g*) for 5 min at 4°C to remove the dead cells from the medium. 20 µg of cell lysate or medium was used to analyze by SDS–PAGE and western blot analysis.

ES cell culture

The G4 ES cell line was grown and manipulated as described previously (48). Briefly, the G4 ES cells were grown and manipulated at 37°C in 5% CO_2 on mitomycin C-treated mouse embryonic fibroblasts [derived from TgN (DR4)1 Jae embryos] in Knockout DMEM (Invitrogen), supplemented with 15% ES FBS (HyClone), 0.1 mM β-mercaptophenol, 2 mM L-glutamine, 1 mM sodium pyruvate, 0.1 mM non-essential amino acids and 2000 U/ml recombinant LIF (DMBR/VIB Protein Service facility).

ES cell electroporation

Two electroporation cuvettes (Biorad) each containing 6×10^6 ES cells resuspended in electroporation buffer (Specialty Media) were electroporated (500 µF, 250 V) with 20 µg of linearized vector. The pROSA-DV2 targeting vector containing the ER-directed GSN Nb11/13 was linearized with *AloI* restriction enzyme (Thermo Scientific, Erembodegem, Belgium). The ES cells were put on ice for 20′ before seeding on a 10 cm dish with mitomycin C-treated mouse embryonic fibroblasts containing ES-cell medium. G418 selection (180 µg/ml) was applied the following day and 7–10 days later, surviving colonies were picked and expanded.

Southern screening

From the surviving colonies after ES cell electroporation, gDNA was isolated and used as template for Southern screening. The gDNA was digested with *EcoRI-HF* and *KpnI* (Bioké, Leiden, The Netherlands). Southern screening was performed as described previously (49). A 5′ external probe was used to identify the ES colonies positive for the GSN nanobody transgene.

ES cell aggregation

Chimeras were generated by aggregation of ROSA26-targeted ES cells with Swiss inner cell mass (ICM) cells. After overnight culture, the resulting blastocysts were transferred to the uteri of pseudo pregnant Swiss fosters. Chimeras were put in test breeding with C57BL/6 mice and the resulting offspring were screened by PCR. Germline offspring were crossed to Sox2-Cre mice to obtain ubiquitous expression of the transgene.

Genotyping and nanobody expression analysis of transgenic mice

For genotype analysis of newborn pups, tail tip amputation was performed and the tail was subsequently lysed overnight in 100 µl DirectPCR Lysis Reagent (Viagen Biotech, Los Angeles, CA, USA) at 55°C, with addition of 1 µl of proteinase K, recombinant PCR grade (Roche, Basel, Switzerland). The next day, the proteinase K was heat inactivated by incubating the lysate at 95°C for 10 min. Centrifugation (29 000*g*) for 5 min was performed to pellet the tail tissue in the lysate. Supernatant (1 µl) was used as template for PCR analysis. Gelsolin amyloidosis genotyping primers: forward 5′ GCAGGAAGACCTGGCAACG 3′, reverse 5′ GGCAACTAGAAGGCACAGTCG 3′. Nanobody genotyping primers: forward 5′ GGATGGAGCTGTATCATCCTCTTCTTGG 3′ and reverse 5′ GCGGCCCCATTCAGATCCTC 3′. For nanobody expression analysis in mouse plasma, blood was collected from the tail vein and centrifuged for 5 min at 4°C (1500*g*). 1 mg of plasma was used for a V5 pull-down experiment as described previously (22). Polyclonal anti-V5 antibody (1:2000) was used for nanobody signal detection.

Mouse plasma and muscle tissue analysis

Mouse plasma (full plasma or albumin cleared) and muscle lysates were obtained and analyzed as described previously (22).

IHC and microscopy

Musculus gastrocnemius tissue was extracted from the hind limb and snap frozen in liquid nitrogen. Cryosections were made and thawed for 15 min. Subsequently, the sections were incubated in aceton for 20 min at −20°C, followed by a quick wash with PBS and 10 min incubation in PBS. Next, sections were incubated in 50 mM NH_4Cl/PBS for 10 min and washed again in PBS. Endogenous peroxidase activity was blocked by incubating in 0.3% H_2O_2 for 20 min followed by washing in PBS. Sections were incubated in 1% BSA/PBS for 20 min and incubated overnight with laminin antibody (1:500) at 4°C. The next day, V5-tagged FAF Nb1 was incubated for 1 h at room temperature at a 5 µg/ml concentration. Next, a PBS wash was performed and secondary antibody (polyclonal anti-V5) was incubated (1:800) for 1 h, followed by a PBS wash. Auto fluorescent antibodies (594 anti-rabbit and 488 anti-mouse; both 1:500) were incubated for 1 h at room temperature. Sections were rinsed in PBS and stained with DAPI (1:500) for 2 min. Finally, sections were mounted with VectaShield and imaged at room temperature using a Leica DM6000 B microscope. Quantification of the images was performed with ImageJ software.

Muscle contractile properties analysis

Performed as described previously (22).

Crystallization and structural determination

Gelsolin G2G3 and Nb11 were mixed in an equal molar ratio in 50 mM Tris–HCl, pH 7.5, and 150 mM NaCl and subjected to size-exclusion chromatography using a HiLoad® 16/60 Superdex® 200 column (GE Healthcare). Eluted fractions of the corresponding complex were then concentrated to 22 mg/ml for crystallization screening at 15°C. A single crystal was observed in a 1:1 ratio sitting drop vapor diffusion condition comprising 30% PEG1500 as precipitant. X-ray diffraction data were collected at the National Synchrotron Radiation Research Center (NSRRC, Taiwan), beamline BL13B1, up to a resolution of 2.6 Å. Data were processed and scaled using the HKL2000 program package (HKL Research). Structural determination was initiated by molecular replacement using a single gelsolin domain from the active N-terminal gelsolin (PDB: 3FFK) and gelsolin nanobody (PDB: 2X1P) structures as search models in PHASER (50). Model building was performed with COOT (51). Restrained refinement of the structure was carried out in the CCP4 suite of programs (52) and PHENIX (53). The

data collection and refinement statistics are listed in Supplementary material, Table S1. All molecular structure figures were generated using PyMOL (Delano Scientific LLC). The atomic coordinates of the G2:Nb11 and Nb11 crystal structures have been deposited into the Protein Data Bank (PDB access 4S10 and 4S11, respectively). Crystals of Nb11 were obtained from 1:1 ratio sitting drop vapor diffusion against 40% PEG8000 in 100 mM HEPES, pH 8.2. X-ray diffraction data were collected at the National Synchrotron Radiation Research Center (NSRRC, Taiwan), beamline BL13B1, up to a resolution of 2 Å (data were processed and scaled using the same programs as for the G2:Nb11 data set.) Structural determination was initiated by molecular replacement using Nb11 from the G2:Nb11 complex.

Statistical analysis

For statistical analysis, two sided unpaired *t*-tests were performed using SPSS software. Data are represented as mean + SE. (*$P < 0.05$; **$P < 0.01$; ***$P < 0.001$).

Supplementary Material

Supplementary Material is available at *HMG* online.

Acknowledgements

We thank L. Haenebalcke, M. Tatari and G. Berx (VIB, IRC, Zwijnaarde) for help with the LR cloning reaction. We thank J.W. Kelly, L.J. Page and A. Guerrero (Scripps Research Institute) for sharing the gelsolin amyloidosis mouse model and L. Supply (Ghent University) for help with immunohistochemistry. We acknowledge B. Vanheel (Dept. of Basic Medical Sciences, Ghent University) for help with muscle contractility experiments. J.W. and R.C.R. thank the Agency for Science, Technology and Research (A*STAR), Singapore for support. Portions of this research were carried out at the National Synchrotron Radiation Research Center, Taiwan. The Synchrotron Radiation Protein Crystallographic Facility is supported by the National Research Program for Genomic Medicine.

Conflict of Interest statement. None declared.

Funding

This work was supported by the Foundation for Alzheimer Research (SAO-FRA), the G.S.K.E. (Geneeskundige Stichting Koningin Elisabeth), the Amyloidosis Foundation (USA), Ghent University (BOF-GOA) and the Interuniversity Attraction Poles Programme of the Belgian State, Federal Office for Scientific, Technical and Cultural Affairs (IUAP P7/13). W.V.O. and A.V. are supported by the Agency for Innovation by Science and Technology in Flanders (IWT-Vlaanderen).

References

1. Harrison, R.S., Sharpe, P.C., Singh, Y. and Fairlie, D.P. (2007) Amyloid peptides and proteins in review. *Rev. Physiol. Biochem. Pharmacol.*, **159**, 1–77.
2. Kirkitadze, M.D., Condron, M.M. and Teplow, D.B. (2001) Identification and characterization of key kinetic intermediates in amyloid beta-protein fibrillogenesis. *J. Mol. Biol.*, **312**, 1103–1119.
3. Walsh, D.M., Hartley, D.M., Kusumoto, Y., Fezoui, Y., Condron, M.M., Lomakin, A., Benedek, G.B., Selkoe, D.J. and Teplow, D.B. (1999) Amyloid beta-protein fibrillogenesis. Structure and biological activity of protofibrillar intermediates. *J. Biol. Chem.*, **274**, 25945–25952.
4. de la Chapelle, A., Tolvanen, R., Boysen, G., Santavy, J., Bleeker-Wagemakers, L., Maury, C.P. and Kere, J. (1992) Gelsolin-derived familial amyloidosis caused by asparagine or tyrosine substitution for aspartic acid at residue 187. *Nat. Genet.*, **2**, 157–160.
5. Meretoja, J. (1973) Genetic aspects of familial amyloidosis with corneal lattice dystrophy and cranial neuropathy. *Clin. Genet.*, **4**, 173–185.
6. Janmey, P.A., Chaponnier, C., Lind, S.E., Zaner, K.S., Stossel, T. P. and Yin, H.L. (1985) Interactions of gelsolin and gelsolin-actin complexes with actin. Effects of calcium on actin nucleation, filament severing, and end blocking. *Biochemistry*, **24**, 3714–3723.
7. Nag, S., Larsson, M., Robinson, R.C. and Burtnick, L.D. (2013) Gelsolin: the tail of a molecular gymnast. *Cytoskeleton*, **70**, 360–384.
8. Nag, S., Ma, Q., Wang, H., Chumnarnsilpa, S., Lee, W.L., Larsson, M., Kannan, B., Hernandez-Valladares, M., Burtnick, L.D. and Robinson, R.C. (2009) Ca2+ binding by domain 2 plays a critical role in the activation and stabilization of gelsolin. *Proc. Natl Acad. Sci. USA*, **106**, 13713–13718.
9. Isaacson, R.L., Weeds, A.G. and Fersht, A.R. (1999) Equilibria and kinetics of folding of gelsolin domain 2 and mutants involved in familial amyloidosis-Finnish type. *Proc. Natl Acad. Sci. USA*, **96**, 11247–11252.
10. Burtnick, L.D., Urosev, D., Irobi, E., Narayan, K. and Robinson, R.C. (2004) Structure of the N-terminal half of gelsolin bound to actin: roles in severing, apoptosis and FAF. *EMBO J.*, **23**, 2713–2722.
11. Chen, C.D., Huff, M.E., Matteson, J., Page, L., Phillips, R., Kelly, J.W. and Balch, W.E. (2001) Furin initiates gelsolin familial amyloidosis in the Golgi through a defect in Ca(2+) stabilization. *EMBO J.*, **20**, 6277–6287.
12. Page, L.J., Suk, J.Y., Huff, M.E., Lim, H.J., Venable, J., Yates, J., Kelly, J.W. and Balch, W.E. (2005) Metalloendoprotease cleavage triggers gelsolin amyloidogenesis. *EMBO J.*, **24**, 4124–4132.
13. Kiuru, S. (1998) Gelsolin-related familial amyloidosis, Finnish type (FAF), and its variants found worldwide. *Amyloid*, **5**, 55–66.
14. Paunio, T., Kangas, H., Kalkkinen, N., Haltia, M., Palo, J. and Peltonen, L. (1994) Toward understanding the pathogenic mechanisms in gelsolin-related amyloidosis: in vitro expression reveals an abnormal gelsolin fragment. *Hum. Mol. Genet.*, **3**, 2223–2229.
15. Kangas, H., Seidah, N.G. and Paunio, T. (2002) Role of proprotein convertases in the pathogenic processing of the amyloidosis-associated form of secretory gelsolin. *Amyloid*, **9**, 83–87.
16. Hamers-Casterman, C., Atarhouch, T., Muyldermans, S., Robinson, G., Hamers, C., Songa, E.B., Bendahman, N. and Hamers, R. (1993) Naturally occurring antibodies devoid of light chains. *Nature*, **363**, 446–448.
17. Delanote, V., Vanloo, B., Catillon, M., Friederich, E., Vandekerckhove, J. and Gettemans, J. (2010) An alpaca single-domain antibody blocks filopodia formation by obstructing L-plastin-mediated F-actin bundling. *FASEB J.*, **24**, 105–118.
18. Van den Abbeele, A., De Clercq, S., De Ganck, A., De Corte, V., Van Loo, B., Soror, S.H., Srinivasan, V., Steyaert, J., Vandekerckhove, J. and Gettemans, J. (2010) A llama-derived gelsolin

single-domain antibody blocks gelsolin-G-actin interaction. *Cell. Mol. Life Sci.*, **67**, 1519–1535.
19. Van Audenhove, I., Van Impe, K., Ruano-Gallego, D., De Clercq, S., De Muynck, K., Vanloo, B., Verstraete, H., Fernandez, L.A. and Gettemans, J. (2013) Mapping cytoskeletal protein function in cells by means of nanobodies. *Cytoskeleton*, **70**, 604–622.
20. Van Impe, K., Bethuyne, J., Cool, S., Impens, F., Ruano-Gallego, D., De Wever, O., Vanloo, B., Van Troys, M., Lambein, K., Boucherie, C. *et al.* (2013) A nanobody targeting the F-actin capping protein CapG restrains breast cancer metastasis. *Breast Cancer Res*, **15**, R116.
21. Muyldermans, S. (2013) Nanobodies: natural single-domain antibodies. *Ann. Rev. Biochem.*, **82**, 775–797.
22. Van Overbeke, W., Verhelle, A., Everaert, I., Zwaenepoel, O., Vandekerckhove, J., Cuvelier, C., Derave, W. and Gettemans, J. (2014) Chaperone nanobodies protect gelsolin against MT1-MMP degradation and alleviate amyloid burden in the gelsolin amyloidosis mouse model. *Mol. Ther.*, **22**, 1768–1778.
23. Seidah, N.G., Day, R., Marcinkiewicz, M. and Chretien, M. (1998) Precursor convertases: an evolutionary ancient, cell-specific, combinatorial mechanism yielding diverse bioactive peptides and proteins. *Ann. N Y Acad. Sci.*, **839**, 9–24.
24. Molloy, S.S., Thomas, L., VanSlyke, J.K., Stenberg, P.E. and Thomas, G. (1994) Intracellular trafficking and activation of the furin proprotein convertase: localization to the TGN and recycling from the cell surface. *EMBO J.*, **13**, 18–33.
25. Molloy, S.S., Bresnahan, P.A., Leppla, S.H., Klimpel, K.R. and Thomas, G. (1992) Human furin is a calcium-dependent serine endoprotease that recognizes the sequence Arg-X-X-Arg and efficiently cleaves anthrax toxin protective antigen. *J. Biol. Chem.*, **267**, 16396–16402.
26. Abrami, L., Fivaz, M., Decroly, E., Seidah, N.G., Jean, F., Thomas, G., Leppla, S.H., Buckley, J.T. and van der Goot, F.G. (1998) The pore-forming toxin proaerolysin is activated by furin. *J. Biol. Chem.*, **273**, 32656–32661.
27. Roebroek, A.J., Umans, L., Pauli, I.G., Robertson, E.J., van Leuven, F., Van de Ven, W.J. and Constam, D.B. (1998) Failure of ventral closure and axial rotation in embryos lacking the proprotein convertase Furin. *Development*, **125**, 4863–4876.
28. Page, L.J., Suk, J.Y., Bazhenova, L., Fleming, S.M., Wood, M., Jiang, Y., Guo, L.T., Mizisin, A.P., Kisilevsky, R., Shelton, G.D. *et al.* (2009) Secretion of amyloidogenic gelsolin progressively compromises protein homeostasis leading to the intracellular aggregation of proteins. *Proc. Natl Acad. Sci. USA*, **106**, 11125–11130.
29. Burtnick, L.D., Koepf, E.K., Grimes, J., Jones, E.Y., Stuart, D.I., McLaughlin, P.J. and Robinson, R.C. (1997) The crystal structure of plasma gelsolin: implications for actin severing, capping, and nucleation. *Cell*, **90**, 661–670.
30. Thomas, G. (2002) Furin at the cutting edge: from protein traffic to embryogenesis and disease. *Nat. Rev. Mol. Cell Biol.*, **3**, 753–766.
31. Zaias, J., Mineau, M., Cray, C., Yoon, D. and Altman, N.H. (2009) Reference values for serum proteins of common laboratory rodent strains. *J. Am Assoc. Lab. Anim. Sci.*, **48**, 387–390.
32. Wolff, S., Weissman, J.S. and Dillin, A. (2014) Differential scales of protein quality control. *Cell*, **157**, 52–64.
33. Guerrero-Munoz, M.J., Castillo-Carranza, D.L. and Kayed, R. (2014) Therapeutic approaches against common structural features of toxic oligomers shared by multiple amyloidogenic proteins. *Biochem. Pharmacol.*, **88**, 468–478.
34. Herva, M.E., Zibaee, S., Fraser, G., Barker, R.A., Goedert, M. and Spillantini, M.G. (2014) Anti-amyloid compounds inhibit alpha-synuclein aggregation induced by protein misfolding cyclic amplification (PMCA). *J. Biol. Chem.*, **289**, 11897–11905.
35. Kisilevsky, R., Ancsin, J.B., Szarek, W.A. and Petanceska, S. (2007) Heparan sulfate as a therapeutic target in amyloidogenesis: prospects and possible complications. *Amyloid*, **14**, 21–32.
36. Molloy, S.S., Anderson, E.D., Jean, F. and Thomas, G. (1999) Bicycling the furin pathway: from TGN localization to pathogen activation and embryogenesis. *Trend. Cell Biol.*, **9**, 28–35.
37. Anliker, B., Abel, T., Kneissl, S., Hlavaty, J., Caputi, A., Brynza, J., Schneider, I.C., Munch, R.C., Petznek, H., Kontermann, R.E. *et al.* (2010) Specific gene transfer to neurons, endothelial cells and hematopoietic progenitors with lentiviral vectors. *Nat. Method.*, **7**, 929–935.
38. Zinn, E. and Vandenberghe, L.H. (2014) Adeno-associated virus: fit to serve. *Curr. Opin. Virol.*, **8**, 90–97.
39. Im, G.I. (2013) Nonviral gene transfer strategies to promote bone regeneration. *J. Biomed. Mat. Res. Part A*, **101**, 3009–3018.
40. Weeds, A.G., Gooch, J., McLaughlin, P. and Maury, C.P. (1993) Variant plasma gelsolin responsible for familial amyloidosis (Finnish type) has defective actin severing activity. *FEBS Lett.*, **335**, 119–123.
41. Maury, C.P. (1993) Homozygous familial amyloidosis, Finnish type: demonstration of glomerular gelsolin-derived amyloid and non-amyloid tubular gelsolin. *Clin. Nephrol.*, **40**, 53–56.
42. Lind, S.E., Smith, D.B., Janmey, P.A. and Stossel, T.P. (1986) Role of plasma gelsolin and the vitamin D-binding protein in clearing actin from the circulation. *J. Clin. Invest.*, **78**, 736–742.
43. Wang, D. and Gao, G. (2014) State-of-the-art human gene therapy: part I. Gene delivery technologies. *Discover. Med.*, **18**, 67–77.
44. Wang, D. and Gao, G. (2014) State-of-the-art human gene therapy: Part II. Gene therapy strategies and clinical applications. *Discover. Med.*, **18**, 151–161.
45. Van den Abbeele, A., De Corte, V., Van Impe, K., Bruyneel, E., Boucherie, C., Bracke, M., Vandekerckhove, J. and Gettemans, J. (2007) Downregulation of gelsolin family proteins counteracts cancer cell invasion in vitro. *Cancer Lett.*, **255**, 57–70.
46. Nyabi, O., Naessens, M., Haigh, K., Gembarska, A., Goossens, S., Maetens, M., De Clercq, S., Drogat, B., Haenebalcke, L., Bartunkova, S. *et al.* (2009) Efficient mouse transgenesis using Gateway-compatible ROSA26 locus targeting vectors and F1 hybrid ES cells. *Nucleic Acids Res.*, **37**, e55.
47. Pasquato, A., Dettin, M., Basak, A., Gambaretto, R., Tonin, L., Seidah, N.G. and Di Bello, C. (2007) Heparin enhances the furin cleavage of HIV-1 gp160 peptides. *FEBS Lett.*, **581**, 5807–5813.
48. George, S.H., Gertsenstein, M., Vintersten, K., Korets-Smith, E., Murphy, J., Stevens, M.E., Haigh, J.J. and Nagy, A. (2007) Developmental and adult phenotyping directly from mutant embryonic stem cells. *Proc. Natl Acad. Sci. USA*, **104**, 4455–4460.
49. Brown, T. (2001) Southern blotting. Current protocols in immunology/edited by John E. Coligan ... [et al.], Chapter 10, Unit 10 16A.
50. McCoy, A.J., Grosse-Kunstleve, R.W., Adams, P.D., Winn, M.D., Storoni, L.C. and Read, R.J. (2007) Phaser crystallographic software. *J. Appl. Crystallogr.*, **40**, 658–674.
51. Emsley, P., Lohkamp, B., Scott, W.G. and Cowtan, K. (2010) Features and development of Coot. *Acta Crystallogr. Sec. D, Biol. Crystallogr.*, **66**, 486–501.

52. Winn, M.D., Ballard, C.C., Cowtan, K.D., Dodson, E.J., Emsley, P., Evans, P.R., Keegan, R.M., Krissinel, E.B., Leslie, A.G., McCoy, A. *et al.* (2011) Overview of the CCP4 suite and current developments. *Acta Crystallogr. Sec. D, Biol. Crystallogr.*, **67**, 235–242.

53. Adams, P.D., Afonine, P.V., Bunkoczi, G., Chen, V.B., Davis, I. W., Echols, N., Headd, J.J., Hung, L.W., Kapral, G.J., Grosse-Kunstleve, R.W. *et al.* (2010) PHENIX: a comprehensive Python-based system for macromolecular structure solution. *Acta Crystallogr. Sec. D, Biol. Crystallogr.*, **66**, 213–221.